J Solid State Electrochem (2005) 9: 574–580
DOI 10.1007/s10008-004-0594-x

ORIGINAL ARTICLE

Haihui Zhou · Hong Chen · Shenglian Luo
Gewu Lu · Wanzhi Wei · Yafei Kuang

The effect of the polyaniline morphology on the performance of polyaniline supercapacitors

Received: 20 February 2004 / Accepted: 15 September 2004 / Published online: 28 January 2005

Abstract The polyaniline (PANI) prepared by the pulse galvanostatic method (PGM) or the galvanostatic method on a stainless steel substrate from an aqueous solution of 0.5 mol/l H_2SO_4 with 0.2 mol/l aniline has been studied as an electroactive material in supercapacitors. The electrochemical performance of the PANI supercapacitor is characterized by cyclic voltammetry, a galvanostatic charge–discharge test and electrochemical impedance spectroscopy in $NaClO_4$ and $HClO_4$ mixed electrolyte. The results show that PANI films with different morphology and hence different capacitance are synthesized by controlling the synthesis methods and conditions. Owing to the double-layer capacitance and pseudocapacitance increase with increasing real surface area of PANI, the capacitive performances of PANI were enhanced with increasing real surface area of PANI. The highest capacitance is obtained for the PANI film with nanofibrous morphology. From charge–discharge studies of a nanofibrous PANI capacitor, a specific capacitance of 609 F/g and a specific energy density of 26.8 Wh/kg have been obtained at a discharge current density of 1.5 mA/cm^2. The PANI capacitor also shows little degradation of capacitance after 1,000 cycles. The effects of discharge current density and deposited charge of PANI on capacitance are investigated. The results indicate that the nanofibrous PANI prepared by the PGM is promising for supercapacitors.

H. Zhou · H. Chen · G. Lu · W. Wei · Y. Kuang (✉)
College of Chemistry and Chemical Engineering,
Hunan University, Changsha,
410082, People's Republic of China
E-mail: yafeik@163.com
Tel.: +86-731-8821259
Fax: +86-731-8713642

S. Luo · W. Wei
State Key Laboratory of Chemo/Biosensing and Chemometrics,
Hunan University, Changsha, 410082, People's Republic of China

Keywords Supercapacitor · Polyaniline · Nanofibrous morphology · Pulse galvanostatic method · Capacitance

Introduction

Supercapacitors (electrochemical capacitors) have attracted much attention in many advanced power systems requiring high power density, high energy density and high cyclability [1–6], such as secondary power sources in electric vehicles to provide peak power for acceleration and hill climbing. Until now, one of the best electrode materials for supercapacitors was an amorphous hydrated ruthenium oxide, which displayed a large specific capacitance value of 760 F/g and excellent cyclability over 100,000 cycles [7, 8]. However, this material is too expensive for commercialization. So, efficient substitutes have been extensively explored, such as activated carbons, NiO and conducting polymers [9–12].

Among all these materials investigated, conducting polymers are the most promising as they possess redox pseudocapacitance in addition to double-layer capacitance. Conducting polymers offer the advantages of low production cost compared with noble metal oxides and high charge capacity compared with activated carbons [13]. So far, the applications of polyaniline (PANI) [13–18], polythiophene [19–22] and polypyrrole [23] in supercapacitors have been reported.

Conducting polymers can be positively or negatively charged with ion insertion in the polymer matrix to balance the injected charge, and hence produce the pseudocapacitance. In the case of PANI, it can be positively charged (p-doped polymer), and both the double-layer capacitance and the pseudocapacitance contribute much to the total capacitance [24]. It is clear that the polymer morphology strongly affects the characterization of a supercapacitor since it influences the specific surface area of the polymer and ion

diffusivity in the polymer matrix during redox switching [14]. Rajendra Prasad and Munichandraiah [24] obtained a specific capacitance value of 815 F/g by potentiodynamical depositing PANI on stainless steel (SS) at high sweep rate (200 mV/s). According to the viewpoint of Rajendra Prasad and Munichandraiah, the high value of the specific capacitance is attributed to a high porous morphology obtained at a high sweep rate for the PANI deposition. Fusalba et al. [14] also considered that it is important to obtain a high-porosity electrode since this kind of morphology is required to achieve material with high ionic conductivity and a capacitor with high energy and power densities. Thus, the performance of PANI supercapacitors may be influenced by the morphology of PANI, which is closely related to the preparation methods and conditions; however, the relationship between the capacitance of PANI and the morphology of PANI has not yet been reported. Talbi et al. [15] constructed a supercapacitor with good cyclability and a high specific capacitance of 230 F/g by combining a porous polyacrylonitrile aerogel with PANI. They considered that a cooperative effect of PANI of a relatively high specific capacitance with a porous polyacrylonitrile aerogel system should give an even larger specific capacitance than just the porous system or the PANI alone. In our recent work, nanofibrous PANI was prepared by a new method called the pulse galvanostatic method (PGM) [25]. This nanofibrous PANI possesses good performance as general conducting polymers, which have high redox pseudocapacitance on account of good doping–undoping ability. Additionally, it has a highly porous structure, a large specific surface area and a high charge-transfer rate, and so it can be used as an excellent electrode material in supercapacitors. We also find that the morphology of PANI varies with the synthesis conditions of the PGM. In the present work, PANI films with different morphology were prepared by various synthesis methods and conditions. The relationship between the morphology of PANI and the capacitance of the PANI/SS electrode is discussed. The capacitive performance of nanofibrous PANI was also investigated. Cyclic voltammetry and electrochemical impedance spectroscopy (EIS) techniques were used to characterize electrochemically the charge capacity of PANI. Galvanostatic charge–discharge cycling of a symmetrical capacitor based on PANI was performed in a two-electrode configuration cell.

Experimental

Chemicals

Aniline was distilled under reduced pressure. The other chemicals used were of analytical grade. All solutions were prepared with double-distilled water.

Preparation of the PANI/SS electrode

Electrochemical depositions were performed in a one-compartment cell using a platinum wire as the counter electrode, a saturated calomel electrode (SCE) as the reference electrode and a SS disk electrode (deposited area 0.95 cm^2) as a working electrode. All potentials were relative to the SCE. A PANI film was prepared by the PGM using an SMD-30 model pulse galvanostant (Handan Instrument Factory, China) from an aqueous solution of 0.5 mol/l H_2SO_4 with 0.2 mol/l aniline. A PANI film was also prepared by the galvanostatic method (GM) using a DHX-II potentiostatic machine (Shenzhen Tonghua Electronic Factory, China) for comparison. For both methods, the current density range was from 2 to 6 mA/cm^2 and the deposited charge range was from 200 to 2,000 mC. For the PGM, the ratio of the "on" pulse period to the "off" pulse period (t_{on}/t_{off}) was 50 ms:50 ms and the frequency was 10 Hz. After deposition, the electrodes were washed free of aniline monomer, and then stored in 1 mol/l $NaClO_4$ and 1 mol/l $HClO_4$ mixed solution until they were used for experiments.

Measurement of anodic polarization of the SS disk

Since SS was used as the substrate for PANI deposition, it is important to study the anodic polarization behavior of bare SS. Anodic polarization was performed using a CHI 660 A electrochemical workstation (Shanghai Chenhua Instrument Factory, China). The potential was between −0.3 and 1.1 V; the sweep rate was 10 mV/s. From the anodic polarization curve in Fig. 1, the SS disk is in a passive state in the potential between −0.3 and 0.8 V.

Measurement of the PANI/SS electrode performance

The CHI 660 A electrochemical workstation was also applied for galvanostatic charge–discharge and EIS

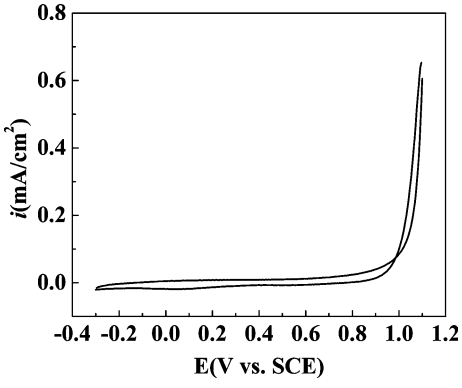

Fig. 1 Cyclic voltammogram of a stainless steel (*SS*) electrode in 1 mol/l $NaClO_4$ and 1 mol/l $HClO_4$ electrolyte at a sweep rate of 10 mV/s

research. The symmetrical capacitor based on PANI was charged/discharged at 1.5 mA/cm^2 between 0 and 0.75 V. EIS was carried out with frequencies varying from 10 kHz to 50 mHz at different cell voltages (ranging from 0 to 0.8 V). All the preparations and measurements were conducted under a N_2 atmosphere at room temperature.

The morphology of PANI was observed using scanning electron microscopy (SEM) with a JSM-5600LV microscope (JEOL Company, Japan).

Results and discussion

The relationship between PANI morphology and capacitive performance

Effect of morphology of PANI prepared by different methods on capacitive performance

While controlling the deposited charge, PANI/SS electrodes were prepared by the PGM and the GM at a mean current density of 2 mA/cm^2. The corresponding SEM images of PANI films are shown in Fig. 2. It can be observed from Fig. 2 that PANI prepared by the PGM shows nanofibrous morphology and PANI prepared by GM shows granular morphology. These results indicate that the morphology of PANI varies greatly with different preparation methods. The possible explanations are described as follows. Although the mean polarized current densities were 2 mA/cm^2 for both the PGM and the GM, $t_{on}/t_{off} = 1$ for the PGM results in an anodic peak current density of the PGM twice that of the polarized current density of the GM, and therefore the polarization behaviors of the polymerization of aniline by the PGM and the GM were obviously different from each other. Meanwhile, the polymerization of aniline may not occur during the "off" pulse period for the PGM and aniline in bulk solution diffuses to the surface of the electrode to supplement the consumption of aniline on the electrode surface for the next periodic reaction, so the transfer of aniline monomer in the vicinity of the electrode surface was apparently different for the PGM and the GM. The corresponding cyclic voltammograms between 0.2 and 0.7 V of the electrodes prepared by these two methods are presented in Fig. 3. The voltammograms of the two electrodes are nearly rectangular in shape without diffusion controlled current peaks, which are in good agreement with those reported by Fusalba et al. [14] and Rajendra Prasad and Munichandraiah [24]. Figure 3 shows that the currents of both the anodic and cathodic half-cycles on PANI/SS electrode prepared by PGM are larger than those on PANI/SS electrode prepared by GM. The integral charge (Q_{int}) can be obtained by integral of current to time in the CVs of Fig. 3. Figure 4 shows the integral charge Q_{int} of PANI/SS capacitors prepared by these two methods. Since Q_{int} was proportional to the capacitance of PANI, it can represent the capacitance of PANI at the same sweep rate. So the PANI/SS capacitor prepared by the PGM has a higher capacitance than the capacitor prepared by the GM with the same deposited charge. This may be attributed to the difference in morphology of PANI prepared by the PGM and the GM. Compared with granular PANI film (Fig. 2), the nanofibrous PANI film has a larger number

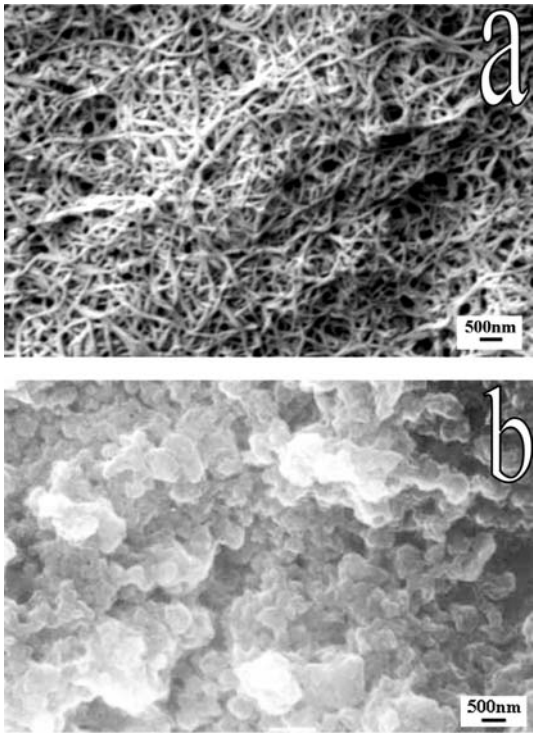

Fig. 2 Scanning electron microscopy images of polyaniline (*PANI*) films prepared by **a** the pulse galvanostatic method (*PGM*) or **b** the galvanostatic method (*GM*) in 0.5 mol/l H_2SO_4 and 0.2 mol/l aniline. PGM conditions: t_{on}/t_{off}, 1:1; frequency, 10 Hz; mean current density, 2 mA/cm^2. GM condition: current density, 2 mA/cm^2

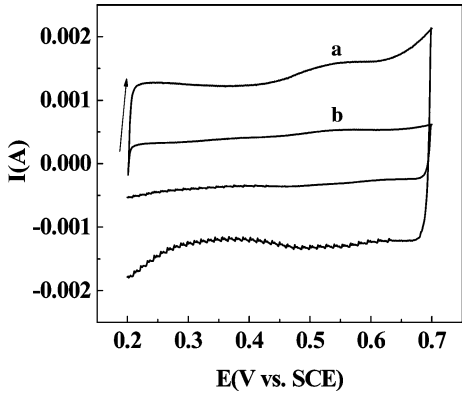

Fig. 3 Cyclic voltammograms of the PANI/SS electrode prepared by the PGM (*a*) and the GM (*b*) in 1 mol/l $NaClO_4$ and 1 mol/l $HClO_4$ electrolyte at a sweep rate of 5 mV/s. PGM conditions: mean current density, 2 mA/cm^2; t_{on}/t_{off}, 1:1; frequency, 10 Hz; Q_{dep}, 2,000 mC. GM conditions: current density, 2 mA/cm^2; Q_{dep}, 2,000 mC

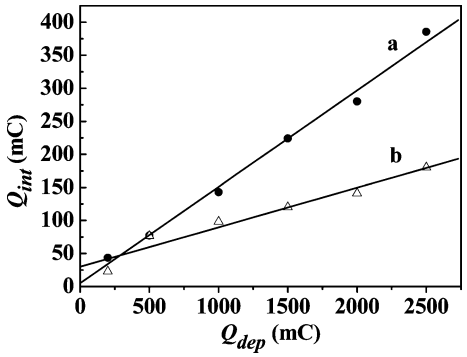

Fig. 4 Comparison of the integral charge (Q_{int}) of PANI/SS prepared by the PGM or the GM (for the PGM, mean current density, 2 mA/cm^2; for the GM, current density, 2 mA/cm^2)

of microgaps and micropores between the fibers. This results in a larger specific surface area and better ionic and electronic conductivity of the film, which result in greater double-layer capacitance and pseudocapacitance. It can be seen from Fig. 4 that the Q_{int} of the PANI/SS capacitor prepared by the PGM is larger than that of the PANI/SS capacitor prepared by the GM at all values of deposited charge. It can also be observed from Fig. 4 that there is an increase in Q_{int} with the increase of the deposited charge for the two capacitors, which implies that the capacitance of PANI increases with the thickness of PANI, but the increase trend in line a is greater than that in line b. From a practical point of view, the PANI loading on the electrode must be as high as possible in order to increase the energy of the capacitor. So the PANI/SS capacitor prepared by the PGM is expected to perform better for capacitor application. That is to say, compared with the GM, the PGM is a superior method to prepare a PANI supercapacitor.

Effect of morphology of PANI prepared by the PGM with different preparation conditions on capacitive performance

SEM images of PANI films prepared by the PGM at different mean current densities are shown in Fig. 5. It can be seen from Figs. 5 and 2a that with the increase of the mean current density, the morphology of the PANI film changes obviously. PANI shows nanofibrous morphology with a fiber diameter of 80–100 nm for a mean current density of 2 mA/cm^2. When the mean current density increases to 6 mA/cm^2, PANI exhibits flake morphology. When the mean current density is 4 mA/cm^2, PANI shows a transitional morphology from nanofibers to flakes. These results indicate that, even using the same preparation method, the morphology of PANI also varies with different preparation conditions. Different mean current densities lead to different pulse peak current densities for preparing PANI films. When $t_{on}/t_{off} = 1$, the pulse peak current densities were 4, 8 and 12 mA/cm^2 with mean current densities of 2, 4 and 6 mA/cm^2, and the corresponding anodic potentials were 0.74, 1.23 and 1.72 V, respectively. It is obvious

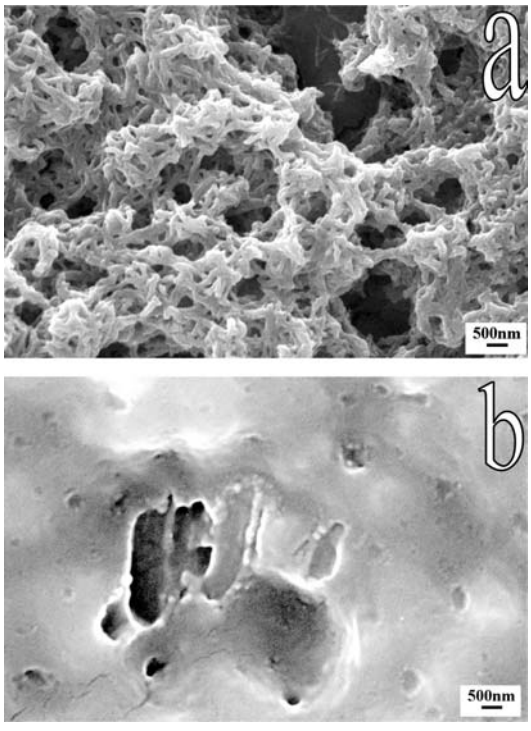

Fig. 5 Scanning electron microscopy images of a PANI film prepared by the PGM in 0.5 mol/l H_2SO_4 and 0.2 mol/l aniline. PGM conditions: t_{on}/t_{off}, 1:1; frequency, 10 Hz; mean current density, **a** 4 mA/cm^2, **b** 6 mA/cm^2

that, when the mean current density was 2 mA/cm^2 (pulse peak current density, 4 mA/cm^2), the potential for preparing PANI was in the normal range, which cannot result in overoxidation of PANI. When the mean current density was 4 mA/cm^2 (pulse peak current density, 8 mA/cm^2), the anodic potential reached 1.23 V, which may slightly cause overoxidation of PANI. When the mean current density was 6 mA/cm^2 (pulse peak current density, 12 mA/cm^2), the anodic potential reached 1.72 V, which certainly causes serious overoxidation of PANI. These were the possible reasons for different PANI morphologies for PANI prepared by the PGM with different mean current densities. Figure 6 presents the influence of the deposited charge (Q_{dep}) on Q_{int} for different morphologies of PANI prepared with various mean current densities. It can be observed from Fig. 6 that Q_{int} decreases with the morphology of PANI varying from nanofibers to flakes. The high capacitance of PANI may result from its nanofibrous morphology, which provides the PANI film with a large specific surface area and is of benefit to the ion diffusion and migration in the PANI film. Hence the double-layer capacitance and pseudocapacitance are improved. In addition, Q_{int} increases with the increase of Q_{dep} when PANI exhibits a nanofibrous or transitional morphology. When PANI shows flake morphology, although the thickness of the PANI film increases with increasing Q_{dep}, the real surface area of the PANI film in contact with the solution does not change much. Consequently,

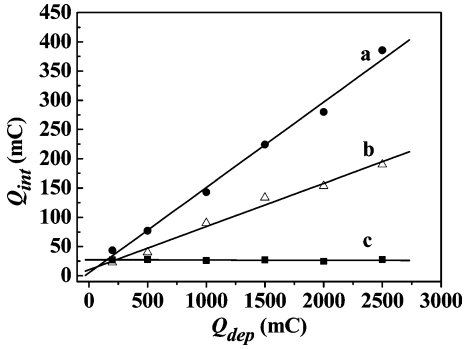

Fig. 6 Influence of the deposited charge (Q_{dep}) and the mean current density of the PGM on the integral charge (Q_{int}) of cyclic voltammetry in 1 mol/l $NaClO_4$ and 1 mol/l $HClO_4$ electrolyte at a sweep rate of 5 mV/s. Mean current densities of 2 mA/cm^2 (*a*), 4 mA/cm^2 (*b*) and 6 mA/cm^2 (*c*)

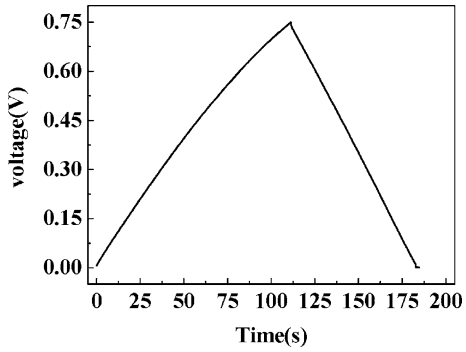

Fig. 7 Typical charge–discharge plot of PANI/SS prepared by the PGM. PGM conditions: mean current density, 2 mA/cm^2; t_{on}/t_{off}, 1:1; frequency, 10 Hz; Q_{dep}, 2,000 mC; charge–discharge current density, 1.5 mA/cm^2

Q_{int} remains almost invariable with the increase of Q_{dep}. These results also indicate that the nanofibrous PANI exhibits better capacitive performance compared with other morphologies of PANI. Meanwhile, the capacitance of nanofibrous PANI increases with increasing thickness of the PANI film. Hence, it can be concluded that the morphology of the conducting polymer was greatly influenced by the preparation methods and preparation conditions. The real surface area of the polymer and the transporting resistance of ions and electrons in the polymer vary with different morphologies, which lead to the difference of the double-layer capacitance and pseudocapacitance of the polymer. Therefore, the polymer used for fabricating electrochemical capacitors should be synthesized by an appropriate preparation method and under appropriate preparation conditions.

The capacitive performance of the nanofibrous PANI/SS capacitor

The specific capacitance and energy density of the nanofibrous PANI/SS capacitor

According to research just described, the nanofibrous PANI/SS capacitor prepared by the PGM exhibits excellent capacitor ability. The galvanostatic charge–discharge test was carried out at various current densities (ranging from 1.5 to 3.5 mA/cm^2) in 1 mol/l $NaClO_4$ and 1 mol/l $HClO_4$mixed electrolyte. Figure 7 shows a representative charge–discharge curve with voltage between 0 and 0.75 V. During the charging step, an almost linear variation of voltage is observed, as expected for a capacitor [6]. During the discharging step, first the electronic conductivity of PANI remains sufficiently high when it is in a high doping state, then undoping reactions of PANI occur and the uncompensated solution resistance leads to an increase in resistance of the capacitor, so the duration of the discharging step is shorter than the charging step. From the curve, the capacitance C_d (farads) is deduced from the slope of the discharging step with

$$C_d = \frac{I}{dV/dt}, \tag{1}$$

where C_d is the capacitance of the PANI/SS capacitor [26], I is the discharge current in amperes, and d V/d t is the slope in volts per second, and the specific capacitance C_{ds}(farads per gram) is related to the capacitance [26]

$$C_{ds} = \frac{C_d}{m}, \tag{2}$$

where m is controlled by the deposited charge—$Q_{dep}(C)$

$$m = \frac{Q_{dep}}{zFM}, \tag{3}$$

where m (grams) is the mass of deposited PANI, and F is the Faraday constant, and M is the molecular weight of aniline, and for the PANI reaction, z is 3 [27].

The influence of Q_{dep} on C_d and C_{ds} of the PANI/SS capacitor is shown in Table 1. A specific capacitance of 609 F/g (charge–discharge current density, 1.5 mA/cm^2) is obtained from Table 1 when the deposited charge is 500 mC. This value is higher than those of an activated carbon electrode [28] and a grainy PANI electrode [29], and is comparable to that of hydrous RuO_2 [7, 8]. Since RuO_2 is much more expensive than PANI, PANI will be more competitive in mass production.

Table 1 Influence of deposited charge (Q_{dep}) on the capacitance (C_d) and specific capacitance (C_{ds}) of the polyaniline/stainless steel capacitor (discharge current density, 1.5 mA/cm^2)

Q_{dep} (mC)	C_d (F)	C_{ds} (F/g)
200	0.036	559
500	0.098	609
1,000	0.169	525
1,500	0.231	479
2,000	0.280	435
2,500	0.313	389

In addition, one can also calculate the energy density of this system using the following equation:

$$E = \frac{CV^2}{2}, \tag{4}$$

where C and V are the specific capacitance (farads per gram) and the operating voltage, respectively [30]. The energy density of the nanofibrous PANI capacitor was found to be 26.8 W h/kg at a specific capacitance of 609 F/g, which is comparable to the energy density of $RuO_2{\cdot}nH_2O$ (26.7 W h/kg) [8].

The life cycle is another important factor for a supercapacitor. The stability of the nanofibrous PANI/SS capacitor prepared by the PGM was evaluated using constant-current cycling over 1,000 continuous charge–discharge cycles. As shown in Fig. 8, the cyclability of the capacitor is excellent, because there is only a marginal decrease of the specific capacitance during 1,000 cycles except for an initial specific capacitance decrease of 60 F/g within 33 cycles. The initial specific capacitance of the PANI/SS capacitor is about 620 F/g and it decreases to 544 F/g at the end.

EIS of the nanofibrous PANI/SS capacitor

Figure 9 presents Nyquist plots at various cell voltages for a freshly prepared nanofibrous PANI supercapacitor assembled with 1 mol/l $NaClO_4$ and 1 mol/l $HClO_4$ electrolyte. The data in Nyquist form show that the system behaves almost like an ideal capacitor at 0 V. It can be seen from Fig. 9 that there is only a relatively small variation in the impedance distribution and in the low-frequency capacitance at different voltages between 0 and 0.5 V. However, when the capacitor voltage reached 0.8 V, the negative electrode was nearly fully reduced. The PANI in the completely reduced state is a poor electronic and ionic conductor. Diffusion-controlled doping and undoping of anions occurs in the positive and negative electrodes, respectively, resulting in Warburg behavior. Therefore, at 0.8 V, when in the low-frequency region, the Nyquist plot does not form an almost 90° linear branch as at a voltage of 0 V. Figure 9 also shows that the high-frequency real impedance component, which corresponds to the solution resistance plus the film electronic and ionic resistances in parallel combination, increases with the increase of capacitor voltage. From the frequency (f*, hertz) corresponding to the maximum of imaginary component (Z'') of the semicircle, the time constant (τ, seconds) of the capacitor is calculated using the following equation:

$$\tau = \frac{1}{2f*}. \tag{5}$$

The value of τ obtained from the data of Fig. 9 is approximately in the range 0.002–0.42 ms. This is lower than that of the PANI/SS capacitor obtained by Rajendra Prasad and Munichandraiah [24]. Low values of τ are preferred for electrochemical capacitors for fast charge–discharge processes [32].

Figure 10 shows impedance spectra for different PANI loadings when the polymer electrode was polarized at 0 V. The high-frequency resistance slightly decreased when less active material is used. This is an expected result, as the electrode is thinner in this case.

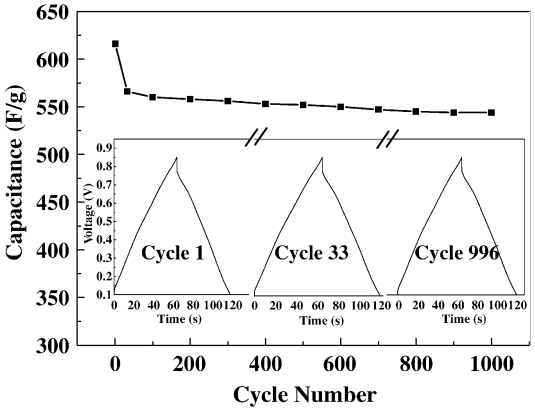

Fig. 8 Life cycle of the PANI capacitor at a current density of 2.5 mA/cm^2. The PANI electrodes were prepared by the PGM to a mass of 0.32 mg/cm^2

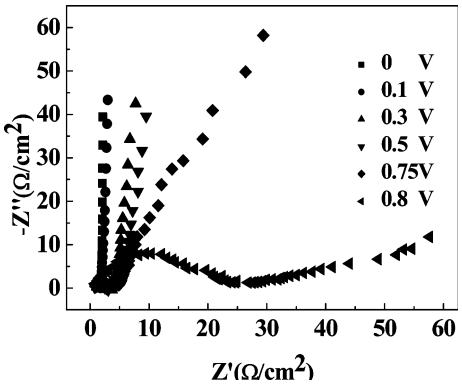

Fig. 9 Nyquist plots of a PANI/SS capacitor at various voltages between 0 and 0.8 V in 1 mol/l $NaClO_4$ and 1 mol/l $HClO_4$ mixed electrolyte. Frequency range, 10 kHz to 50 mHz. Deposited charge, 1,000 mC

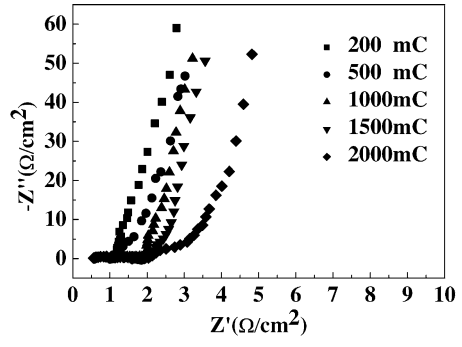

Fig. 10 Nyquist plots of a PANI/SS capacitor at various deposited charges between 200 and 2,000 mC in 1 mol/l $NaClO_4$ and 1 mol/l $HClO_4$ mixed electrolyte. Frequency range, 10 kHz to 50 mHz. Cell voltage, 0 V

The most important difference occurs in the medium-frequency range, i.e., where the electrode thickness and porosity effects can be seen. When the electrode thickness increases (with greater amount of active material), the shift toward more positive resistance values increases owing to the higher ionic and electronic resistance of the thicker polymer film electrode.

Conclusion

PANI films with different morphologies were prepared by the PGM and the GM, and the corresponding capacitive performance of PANI with different morphologies was investigated. The results show that, compared with granular or flake PANI, nanofibrous PANI has better capacitive performance. This is mainly on account of the larger real surface area and the better electronic and ionic conductivity of nanofibrous PANI, which lead to greater double-layer capacitance and faradic pseudocapacitance. The research on the capacitive performance of nanofibrous PANI also shows that the nanofibrous PANI capacitor prepared by the PGM yields a high specific capacitance of about 609 F/g in 1 mol/l $NaClO_4$ and 1 mol/l $HClO_4$ and a specific energy density of 26.8 W h/kg at a discharge current density of 1.5 mA/cm^2. The nanofibrous PANI supercapacitor also shows high stability during long cycles. The PGM is a good method to synthesize nanofibrous PANI, which is promising for application as a supercapacitor.

Acknowledgements This work was supported by the National Natural Science Foundation of China (No. 50473022) and the foundation of State Key Laboratory of Chemo/Biosensing and Chemometrics of China.

References

1. Lin C, Ritter JA, Popov BN (1999) J Electrochem Soc 146:3155
2. Zheng JP (1999) Electrochem Solid State Lett 2:359
3. Miller JM, Dunn B, Tran TD, Pekala RW (1997) J Electrochem Soc 144:L309
4. Conway BE (1991) J Electrochem Soc 138:1539
5. Conway BE, Birss V, Wojtowicz J (1997) J Power Sources 66:1
6. Conway BE (1999) Electrochemical supercapacitors: scientific fundamentals and techological applications. Kluwer/Plenum, New York
7. Zheng JP, Jow TR (1995) J Electrochem Soc 142:L6
8. Zheng JP, Jow TR (1996) J Power Sources 62:155
9. Liu KC, Anderson MA (1996) J Electrochem Soc 143:124
10. Lee HY, Goodenough JB (1999) J Solid State Chem 144:220
11. Pang SC, Anderson MA, Chapman TW (2000) J Electrochem Soc 147:44
12. Barsukov V, Chivikov S (1996) Electrochim Acta 41:1773
13. Belanger D, Ren X, Davey J, Uribe F, Gottesfeld S (2000) J Electrochem Soc 147:2923
14. Fusalba F, Gouerec P, Villers D, Belanger D (2001) J Electrochem Soc 148:A1
15. Talbi H, Just P-E, Dao LH (2003) J Appl Electrochem 33:465
16. Langer JJ, Krzyminiewski R, Kruczynski Z, Gibinski T, Czajkowski I, Framski G (2001) Synth Met 122:359
17. Hu CC, Chu CH (2001) J Electroanal Chem 503:105
18. Varela H, Maranhao SLA, Mello RMQ, Ticianelli EA, Torresi RM (2001) Synth Met 122:321
19. Rudge A, Raistrick I, Gottesfeld S, Ferraris JP (1994) Electrochim Acta 39:273
20. Ferraris JP, Eissa MM, Brotherston ID, Loveday DC, Moxey AA (1998) J Appl Electrochem 459:57
21. Laforgue A, Simon P, Sarrazin C, Fauvarque JF (1999) J Power Sources 80:142
22. Mastragostino M, Arbizzani C, Soavi F (2001) J Power Sources 97–98:812
23. Frackowiak E, Jurewicz K, Delpeux S, Beguin F (2001) J Power Sources 97–98:822
24. Rajendra Prasad K, Munichandraiah N (2002) J Electrochem Soc 149:A1393
25. Jiao SQ, Peng XH, Zhou HH, Chen JH, Kuang YF (2003) Chem J Chin Univ 24:1118
26. Taberna PL, Simon P, Fauvarque JF (2003) J Electrochem Soc 150:A292
27. Stilwell DE, Park SM (1988) J Electrochem Soc 135:2254
28. Morimoto T, Hiratsuka K, Sanada Y (1996) J Power Sources 60:239
29. Rajendra Prasad K, Munichandraiah N (2002) Electrochem Solid State Lett 5:A271
30. Hong MS, Lee SH, Kim SW (2002) Electrochem Solid State Lett 5:A227
31. Lin CQ, Popov BN, Ploehn HJ (2002) J Electrochem Soc 149:A167
32. Burke AFJ (2000) Power Sources 91:17